Spin density wave and superconducting properties of nanoparticle organic conductor assemblies

Laurel E. Winter, Eden Steven, James S. Brooks, Shermane Benjamin, Ju-Hyun Park, Dominique de Caro, Christophe Faulmann, Lydie Valade, Kane Jacob, Imane Chtioui, Belén Ballesteros, and Jordi Fraxedas

Spin density wave and superconducting properties of nanoparticle organic conductor assemblies

Laurel E. Winter,[1, *] Eden Steven,[1, †] James S. Brooks,[1] Shermane Benjamin,[1]
Ju-Hyun Park,[2] Dominique de Caro,[3, 4] Christophe Faulmann,[3, 4] Lydie Valade,[3, 4]
Kane Jacob,[3, 4] Imane Chtioui,[3, 4] Belén Ballesteros,[5, 6] and Jordi Fraxedas[5, 6]

[1]*Department of Physics and National High Magnetic Field Laboratory,*
Florida State University, Tallahassee, FL 32310, USA
[2]*National High Magnetic Field Laboratory, Florida State University, Tallahassee, FL 32310, USA*
[3]*CNRS, LCC (Laboratoire de Chimie de Coordination),*
205 route de Narbonne, BP 44099, 31077 Toulouse Cedex 4, France
[4]*Université de Toulouse, UPS, INPT, 31077 Toulouse Cedex 4, France*
[5]*ICN2 - Institut Catala de Nanociencia i Nanotecnologia,*
Campus UAB, 08193 Bellaterra (Barcelona), Spain
[6]*CSIC - Consejo Superior de Investigaciones Cientificas,*
ICN2 Building, 08193 Bellaterra (Barcelona), Spain
(Dated: January 6, 2015)

The magnetic susceptibilities of nanoparticle assemblies of two Bechgaard salts, $(TMTSF)_2PF_6$ and $(TMTSF)_2ClO_4$, have been studied vs. temperature and magnetic field. In the bulk these materials exhibit a spin density wave formation ($T_{SDW} = 12$ K) and superconductivity ($T_c = 1.2$ K), respectively. We show from inductive (susceptibility) measurements that the nanoparticle assemblies exhibit ground state phase transitions similar to those of randomly oriented polycrystalline samples of the parent materials. Resistivity and diamagnetic shielding measurements yield additional information on the functional nanoparticle structure in terms of stoichiometric and non-stoichiometric composition.

I. INTRODUCTION

Restricted geometries have been realized in many materials such as semiconductors and metals, and often the bulk properties are modified when the size of a structure approaches the characteristic extent of the ground state order parameter. For instance, in semiconductor devices[1] or type I elemental metal superconductors like aluminum[2,3] the evolution from an insulator to a metal or superconductor is observed with increasing electron density or film thickness, and in nanoparticles of tin[4] or lead[5,6] a modification of the superconducting properties is observed for sizes smaller than the coherence lengths. The single molecule magnet material Mn_{12}-acetate has also been produced as a thin film[7]. Although the film retains aspects of the more dramatic magnetic hysteresis effects seen in the bulk crystalline materials, modifications such as an additional magnetic phase also appear. However, progress in the study of thin film and nanoparticle geometries in the important class of organic superconductors, which are predominantly charge transfer organic salts with relatively large donor and acceptor organic molecules, has remained elusive. This is due to the reluctance of these materials to naturally form epitaxial layers on substrates – rather, the default growth morphology, for instance via electrocrystallization, is often the nucleation of small crystallites at arbitrary orientations. Some progress has been made by evaporation/sublimation methods that produce small patches of ordered charge transfer complexes on metallic substrates that can then be measured by scanning probe methods[8]. Such sample geometries and measurements present considerable challenges, and are not conducive to other characterization methods that can probe the ground state thermodynamics of a nanostructure.

Recently dispersed nanoparticles of donor-acceptor (DA) organic conductors have been synthesized by either oxidation or electrocrystallization in the presence of stabilizing agents acting as growth inhibitors[9]. Additional refinements of the synthesis conditions have produced a number of DA organic superconductors where strong correlations between the spectroscopic and crystallographic properties of the bulk materials and the nanoparticles have been established[10]. In light of these advances, the main purpose of the present work is to identify the low temperature thermodynamic ground states of the nanoparticle species. An example of the nanocrystalline and nanoparticle structure of $(TMTSF)_2ClO_4$ is shown in Fig. 1. High resolution transmission electron microscope (HR-TEM) studies[10] show that single crystal constituent nanoparticles of approximately 3 to 5 nm in size (see Supplementary Figure 1[11]) make up nanoparticles that TEM images show are on average about 10 times larger (e.g. average cluster size of 34 nm). These nanoparticles form a fine powder (assembly) with a random crystallographic orientation (see Supplementary Figure 2[11]) that is then used for the characterization of the physical properties.

We focus on the low temperature and high magnetic field properties of two new nanoparticle systems in the class of the Bechgaard salts[12]. The first is $(TMTSF)_2PF_6$ (also, NP-PF$_6$) which undergoes a spin density wave (SDW) and metal-insulator transition at $T_{SDW} = 12$ K, and the second is $(TMTSF)_2ClO_4$ (also, NP-ClO$_4$) which, due to the low symmetry of the tetrahedral an-
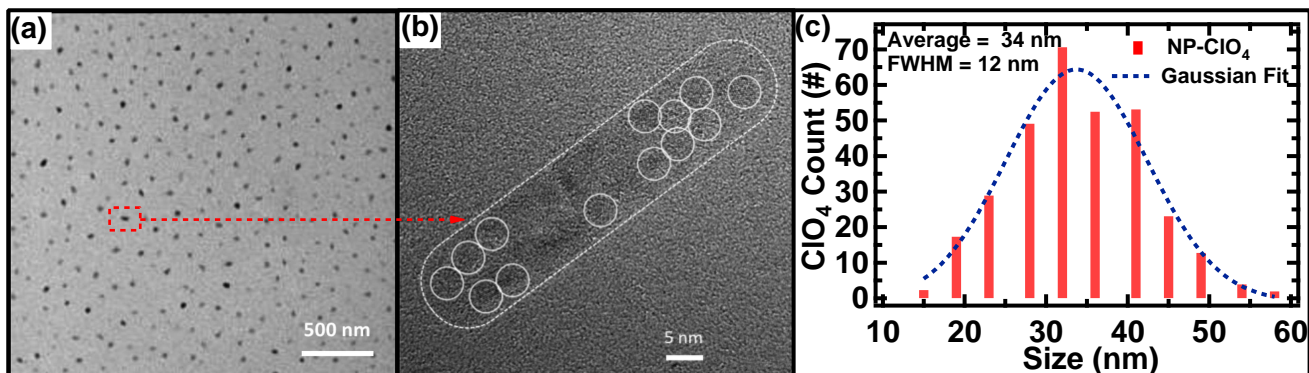
FIG. 1. $(TMTSF)_2ClO_4$ nanoparticles. (a) Low resolution TEM image of nanoparticles dispersed on a substrate. (b) HR-TEM image of nanoparticle structure: dashed envelope, approximate extent of the overall nanoparticle; circles, positions of constituent nanoparticles of 3 to 5 nm in size. (c) Size distribution of nanoparticles in (a). Nanoparticles of $(TMTSF)_2PF_6$ exhibit similar morphologies and size distributions

ion ClO_4, first undergoes an anion ordering transition at $T_{AO} = 24$ K, followed by a superconducting transition at $T_c = 1.2$ K[13]. The main goal of the present work is to determine if the nanoparticle morphologies of these materials exhibit the same ground states as the bulk single crystalline materials. We will show that the ground state properties of the nanoparticles compare favorably with their bulk counterparts when the highly anisotropic nature[14]of the Bechgaard salt properties are taken into account. (Bulk crystals form in needle-like morphologies where the most conducting axis is the a-axis oriented along the needle direction, the a-b plane constitutes a conducting layer, and the c-axis is the least conducting direction, normal to the layers.) However, an unambiguous demonstration of a possible alteration of the bulk ground state properties when the nanoparticle size is less than the ground state coherence lengths will require further studies.

II. RESULTS AND DISCUSSION

For clarity in terminology in what follows, we note that the objects on the order of 30 to 60 nm as seen in the lower resolution TEM image (Fig. 1a) are referred to as *nanoparticles*. These nanoparticles are made up of smaller entities, referred to as the *constituent nanoparticles*, with size 3 to 5 nm as seen from the HR-TEM image (Fig. 1b). For susceptibility and inductive studies, the samples measured were encapsulated *powders* or *assemblies* (see Supplementary Figure 2[11]) comprised of nanoparticles. For electrical transport measurements, nanoparticle assemblies were studied in a four-terminal configuration. In the following sections measurements on the nanoparticle assemblies are presented in parallel with comparisons with bulk single crystal results. Since the Bechgaard salts are highly anisotropic in terms of their electronic structure and magnetic field effects[12], a comparison of the electronic properties and susceptibility of a

randomly oriented assembly of nanoparticles (and therefore the constituent nanoparticles) with previous bulk single crystal measurements requires an average of the a, b and c-axis properties. For this purpose, we assume that the electrical current path or applied magnetic field direction lies with equal probability along any of the three principle axes of each nanoparticle. This leads to a simple 1/3 contribution of the property from each direction, averaged to allow a comparison with the corresponding nanoparticle assembly data.

A. Spin density wave transition in $(TMTSF)_2PF_6$ nanoparticles

We first discuss the electronic transport of the SDW transition in the $(TMTSF)_2PF_6$ nanoparticle assembly. In powders, the nanoparticles tend to form a dense, interconnected assembly unlike that observed in crushed single crystal powders where the crystals are well dispersed and separated (Supplementary Figure 2[11]). This indicates a strong interparticle interaction between nanoparticles (Supplementary Video 1[11]). The source of this unusual mutual attraction is not presently understood, but based on the sample preparation we do not believe there are residual solvents or stabilizing agents on the surface of the nanoparticles. We find the assembly is electrically conducting, and the temperature dependent resistance of the nanoparticle assembly was studied using an adhesive stamp electrode method[15] and a lock-in amplifier (SRS 830) in a 4-probe configuration down to cryogenic temperatures. As observed in Fig. 2, the SDW transition (accompanied by a metal-insulator transition) occurs at $T_{SDW} = 12$ K, similar to that of the bulk single crystals. We note that in bulk single crystals, the temperature dependent resistance above T_{SDW} is metallic, i.e. $dR/dT > 0$, but the nanoparticle assembly shows very little dependence of the resistance above T_{SDW}. However, below T_{SDW} the activated component of the resistance rises
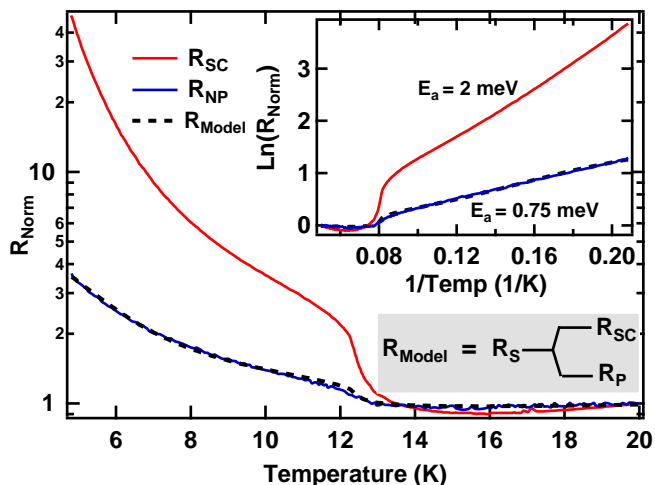
FIG. 2. Electrical transport in the $(TMTSF)_2PF_6$ nanoparticle (NP) assembly compared with single crystal (SC) (*c*-axis) measurements. Upper inset: Comparison of Arrhenius activation plots for the nanoparticle assembly and single crystals showing the lower activation energy for the nanoparticle assembly. Lower insert sketch: Series (R_S) & parallel (R_P) model for the nanoparticle assembly resistance.

quickly and is clearly observable above the background.

Notably, the activation energy (E_a) of the NP-PF$_6$ assembly is much lower compared to the case for a bulk single crystal (Fig. 2, upper inset). In the simplest case, this lower E_a can be assigned to the presence of non-stoichiometric contributions to the overall transport signal. If the electrical transport in the NP-PF$_6$ assembly (R_{NP}) is purely stoichiometric, then the activation energy should be close to that seen in a single crystal. However, if there are non-stoichiometric resistances in series (R_S) and parallel (R_P) to the stoichiometric resistance (R_{SC}), then the temperature dependence of the transport will be modified. We have used a simple series-parallel model (Fig. 2, lower inset) to describe the apparent suppression of E_a. Our model assumes that each nanoparticle in a compacted assembly is separated from the others by a thin non-stoichiometric coating. Hence the coating will give rise to both series (R_S) and parallel (R_P) resistances with respect to the stoichiometric resistance R_{SC}. We further assume the non-stoichiometric resistances are constant with the temperature, and the stoichiometric resistance R_{SC} follows the temperature dependence of a bulk single crystal (which is small above T_{SDW}, and rises rapidly below T_{SDW}). For the analysis, we have normalized the resistances to the data at 20 K and included a weighting ratio, η, which represents the portion of the total resistance that is due to parallel elements in the circuit. The model for the temperature dependence of the total resistance of the assembly is $R_{Model} = (1 - \eta)*R_S + \eta*[R_{SC}*R_P/(R_{SC} + R_P)]$. It provides an excellent fit to the experimental data (Fig. 2 upper inset), where we find $\eta = 0.2$, $R_S = 1$, and $R_P = 19.1$. This means that at most the stoichiometric contribution to the overall re-

sistance of the NP-PF$_6$ assembly is 20% of R_{SC} (in the limit that $R_P \rightarrow \infty$). The rest is due to contributions that could originate from some combination of contact resistances between individual nanoparticles and/or non-stoichiometric material.

The main results of this analysis are that for the self-adhering powdered nanoparticle assembly of $(TMTSF)_2PF_6$, electrical conductivity occurs via a combination of transport through stoichiometric and non-stoichiometric material in effectively parallel and series pathways. This implies that the effective activation energy in the SDW state (of the stoichiometric material) will be reduced by the presence of conduction through non-stoichiometric parallel pathways. It also indicates the contribution of the stoichiometric resistance becomes most evident below the SDW transition where its resistance rises by orders of magnitude with respect to the non-stoichiometric material.

Next, we examine the magnetic susceptibility χ of the SDW transition in $(TMTSF)_2PF_6$ nanoparticles shown in Fig 3a. To study the magnetic properties, NP-PF$_6$ powders of mass 63.8 mg were placed in a polycarbonate capsule and measured in a commercial superconducting susceptometer (MPMS-Quantum Design) vs. temperature and magnetic field. The background signal from the polycarbonate capsule was measured independently. The spin susceptibility is obtained by subtracting the molecular diamagnetism[16] $\chi_{mol} = 3.5 \times 10^{-4}$ emu/mol of $(TMTSF)_2PF_6$ from the total susceptibility. For comparison (Fig. 3b), the most complete previous study of the anisotropic susceptibility for a bulk single crystal was in the isostructural material $(TMTSF)_2AsF_6$ (with nearly identical properties) reported by Mortensen *et al.*[16] for the *a*, *b*, and *c* directions with respect to an applied field of H = 0.3 T. It was found that below T_{SDW} = 12 K, χ_b dropped rapidly, indicating antiferromagnetic order develops along the *b*-axis. In contrast, χ_a and χ_c remain paramagnetic below T_{SDW}. It was further found (Fig. 3c) that a magnetic field applied along the *b*-axis induces a spin-flop at $H_{sf} \approx 0.45$ T, where χ_b then approaches χ_a and χ_c.

From Figs. 2 and 3 it is clear that the $(TMTSF)_2PF_6$ nanoparticle assembly exhibits qualitatively the same SDW ground state of a bulk single crystal, including the metal insulator transition and the spin-flop behavior in magnetic field compared with a simple averaging argument based on bulk single crystal results. There is no apparent shift in the SDW transition temperature between the nano and bulk materials, indicating that the effective coherence length (ξ) of the SDW order parameter is comparable to or smaller than the effective nanoparticle size (estimated from a simple BCS type argument to be $\xi = \hbar\nu_F/2\pi k_B T_{SDW} \approx 10$ nm). Qualitatively, in Fig. 3 there may be some functional differences in the field and temperature dependence of the nanoparticle susceptibility and in the higher spin-flop saturation (1.5 T vs. 0.45 T), but at present we cannot make any significant assignment of the behavior to size effects.
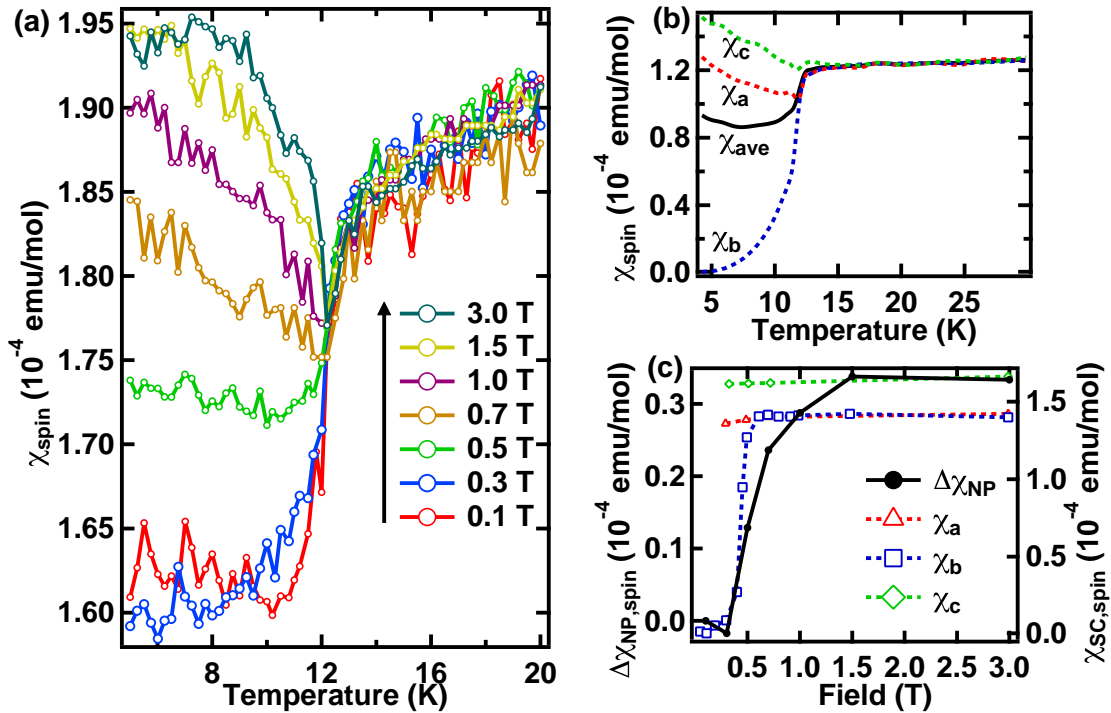
FIG. 3. Magnetic properties of $(TMTSF)_2PF_6$. (a) Temperature and magnetic field-dependent susceptibility of a randomly oriented $(TMTSF)_2PF_6$ nanoparticle assembly. The curves have been shifted to coincide with the 3 T data at 13 K to account for a systematic field-dependent background. (b) Single crystal results for $(TMTSF)_2AsF_6$ from Ref. 16 for a, b and c-axis orientations at 0.3 T. The solid line is a simple average of the susceptibility for all three directions (compare with 0.3 T data in Fig. 3a). (c) Spin-flop behavior at 5 K (left axis: $\Delta\chi_{NP} = \chi_{NP}(5\ K, B) - \chi_{NP}(5\ K, 0.1\ T)$) compared with χ_b results for single crystal $(TMTSF)_2AsF_6$ from Ref. 16 (right axis: χ_a, χ_b, χ_c), where we note that the field dependences of χ_a and χ_c are negligible on this scale.

B. Superconductivity and critical magnetic fields in $(TMTSF)_2ClO_4$ nanoparticles

We next turn our attention to the $(TMTSF)_2ClO_4$ nanoparticle system. Due to the low temperature of the superconducting transition temperature ($T_c = 1.2$ K) in $(TMTSF)_2ClO_4$, which was below the 1.5 K limit of the MPMS, we used a high sensitivity inductive method in a dilution refrigerator in a 16 T superconducting magnet to study the diamagnetic signal associated with the superconducting state. (The superconducting magnet was swept through zero magnetic field to eliminate remnant field effects due to trapped flux in the solenoid.) The inductive method involves a tunnel diode oscillator (TDO) self-resonating LC circuit (L = inductor, C = capacitor) operating with a frequency f and driven by a tunnel diode biased in the negative resistance region[17,18]. Changes in the resonant frequency are directly proportional to any mechanism that changes the effective inductance of a coil in which the sample is placed. In the case of a superconducting transition, this occurs due to the diamagnetic response that effectively reduces the volume of the coil due to flux excluded from the sample, leading to an increase in the resonant frequency. For this work, an assembly of NP-ClO_4 of mass 7.385 mg (corresponding to a sample

volume of 3.1 mm^3) was placed inside a non-magnetic gelatin capsule with an approximate capsule volume of 18.08 mm^3, which was then placed inside of a 40 turn coil (L) with an approximate length and volume of 4.6 mm and 23.68 mm^3, respectively. The rms field (h) due to the measurement coil is estimated to be 0.04 Oe, well below the lower (Meissner) critical field H_{c1} for $T < T_c$. For comparison with the superconducting diamagnetic signal χ_d obtained by conventional methods, we present our results as the temperature dependent change in the resonant frequencies $f(T_c) - f(T) \equiv -\delta f(T) \sim -\chi_d$.

We note that in preparation for the low temperature measurements, the nanoparticle assembly was cooled very slowly (< 0.1 K/min) through the anion ordering transition $T_{AO} = 24$ K in order to avoid quenching[19,20]. The absolute change in the TDO frequency as a function of temperature for the NP-ClO_4 assembly, with no external applied magnetic field, is shown in Fig. 4. A decrease in $-\delta f$ is observed starting at approximately 1.2 K due to the diamagnetic onset of the superconducting transition that approaches a minimum around 0.03 K, the lowest temperature available for this study. The frequency shift data in Fig. 4 is characteristic of the response of a superconductor below T_c for which the decrease in the susceptibility $\chi(T)$, penetration depth $\lambda(T)$ or the inductive signal $-\delta f$ are equivalent indications of the ex-
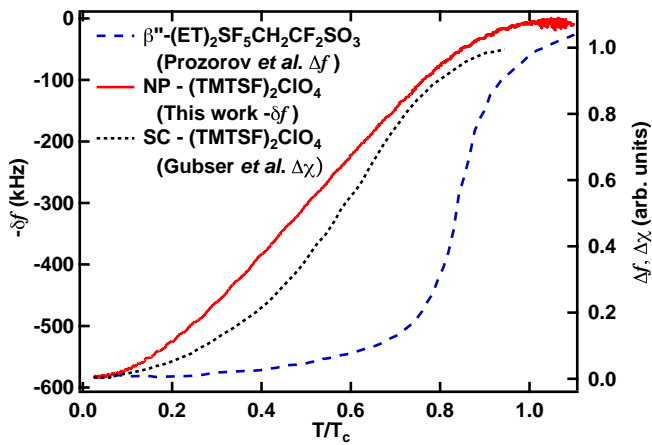
FIG. 4. A comparison between the change in frequency (-δf) for $(TMTSF)_2ClO_4$ nanoparticles ($T_c \sim 1.2$ K), the normalized average relative susceptibility ($\Delta\chi$) of a bundle of $(TMTSF)_2ClO_4$ single crystals ($T_c \sim 1.1$ K) by Gubser *et al.*[21], and the averaged penetration depth change (Δf) of β''-$(ET)_2SF_5CH_2CF_2SO_3$ ($T_c \sim 5.5$ K)[22] as a function of reduced temperature T/T_c.

cluded sample volume due to diamagnetic shielding currents. The results for -δf are in qualitative agreement with previous susceptibility measurements performed by Gubser *et al.*[21] for a bundle of aligned crystals (Fig. 4). The weak, sigmoidal nature of the temperature dependence of -δf in Fig. 4 does not correspond to the much stronger temperature dependence of a BCS-type model $\lambda(T) = \lambda(0)*(1 - (T/T_c)^\gamma)^{-1/2}$ where the exponent (typically between 1.5 and 4) depends on the nature of the superconducting order parameter. This is made evident by comparison with another organic superconductor, β''-$(ET)_2SF_5CH_2CF_2SO_3$[22] where the rise in $\lambda(T)$ (Δf in the Fig. 4) near T_c (~ 5.5 K) is rapid. Due to the layered, anisotropic structure of organic superconductors, the orientation of the sample in the inductor coil plays a significant role. Defining the layers to lie in the a-b plane, for the oscillating magnetic field h perpendicular to the c-axis, $\lambda_\perp(T)$ can be much larger and less temperature dependent than $\lambda_\parallel(T)$ for h parallel to the c-axis. A simple averaging to find the contributions for the a, b, and c directions in β''-$(ET)_2SF_5H_2CF_2SO_3$ merely reduces the range, but not the temperature dependence of Δf.

The shielding fraction of the NP-ClO_4 assembly may be estimated from the experimental parameters. To facilitate the discussion, a model of the NP-ClO_4, to be discussed below, is presented in Fig. 5. Following on the analysis for NP-PF_6, we assume that there is a stoichiometric nanoparticle core surrounded by non-stoichiometric material; their sum makes up the total mass (and volume) of the nanoparticle.

The total nanoparticle assembly volume, based on the mass of the assembly, is $V_{assem.} = 3.1$ mm^3, and the volume of the inductor coil is $V_{coil} = 23.68$ mm^3. The TDO resonant frequency is $f_0 = A V_{coil}^{-1/2}$ (where A

is a constant dependent on physical constants and geometrical factors). If a superconducting sample is placed in the coil, then the altered frequency due to an effective shielded volume V_s due to diamagnetic currents will be $f_s = A(V_{coil} - V_s)^{-1/2}$. Using Figs. 4 and 5a we may estimate V_s at 0.03 K from the simple relationship $(V_{coil} - V_s)/V_{coil} = (f_0/f_s)^2$, where $f_s - f_0 = -\delta f(0.03$ K$)$. We find that $V_s = 0.075 * V_{coil} = 1.79$ mm^3, which implies that at 0.03 K, about 58% of nanoparticle material is superconducting and shields the field. Therefore 42% of the nanoparticle assembly volume is either penetrated by field or is non-stoichiometric material. There are two different scenarios of how the nanoparticle assembly can act: a) the nanoparticles are either electrically connected or Josephson coupled, acting as a monolithic solid body where the shielding currents appear at the periphery (Fig. 5a); b) as an assembly of weakly interacting nanoparticles (Fig. 5b) where the field easily penetrates, and the diamagnetic shielding arises from the sum of individual superconducting nanoparticles[23].

Scenario (a): If we assume that there is no non-stoichiometric material (i.e. $r_{stoich.} = r_{assem.}$), we may estimate how far the magnetic field penetrates into the nanoparticle assembly volume at low temperature, i.e. the effective change in penetration depth $\Delta\lambda_{eff} = \lambda(T_c) - \lambda(T = 0)$ by assuming $\lambda(T_c) \sim r_{assem.}$ for a spherical sample shape of radius $r_{assem.}(\equiv [\frac{3}{4}\pi V_{assem.}]^{1/3})$, and shielded sample radius $r_s(\equiv [\frac{3}{4}\pi V_s]^{1/3})$. Using the relation $\frac{4}{3}\pi(r_{assem.} - \Delta\lambda_{eff})^3 = V_s$ we find $\Delta\lambda_{eff} \sim 150$ μm. If there is non-stoichiometric material, then $\Delta\lambda_{eff}$ will be smaller. We note that $\Delta\lambda_{eff} \sim 150$ μm is in the range of values for the penetration depth reported for other organic superconductors, ($\lambda_\perp \sim 800$ μm and $\lambda_\parallel \sim 1$ μm for anisotropic β''-$(ET)_2SF_5CH_2CF_2SO_3$[22]), and that it is significantly larger than the range of coherence lengths in $(TMTSF)_2ClO_4$: 80 nm $< \xi <$ 2 nm.

Scenario (b): The nanoparticles act individually. Noting that the rms ac field $h = 0.04$ Oe $<<$ H_{c1}, no vortex state enters an individual nanoparticle, and since λ (microns) $>> \xi \sim$ nanoparticle size (nanometers), the presence of the field would result solely in a reduced superconducting order parameter within the nanoparticle[24], and the diamagnetic response would come from the sum of the nanoparticles in the assembly, mimicking a bulk solid body response. Previous work on Pb nanoparticles indicates that even in a compacted state, the nanoparticles act as individual entities[5] and give rise to a bulk-like diamagnetic signal. Moreover, there is no suppression in T_c until the nanoparticle size is only about 10% of the bulk coherence length.

We next turn to the magnetic field dependence, determined systematically by isothermal magnetic field sweeps for temperatures between 1.5 K and 33 mK. Shown in Fig. 6 are the normalized changes in the TDO frequency δf_{norm}, which is normalized with respect to -δf at zero field for the lowest temperature sweep (T = 33 mK, see Supplementary Figure 3[11]), for increasing magnetic field for two representative temperatures below $T_c \sim$
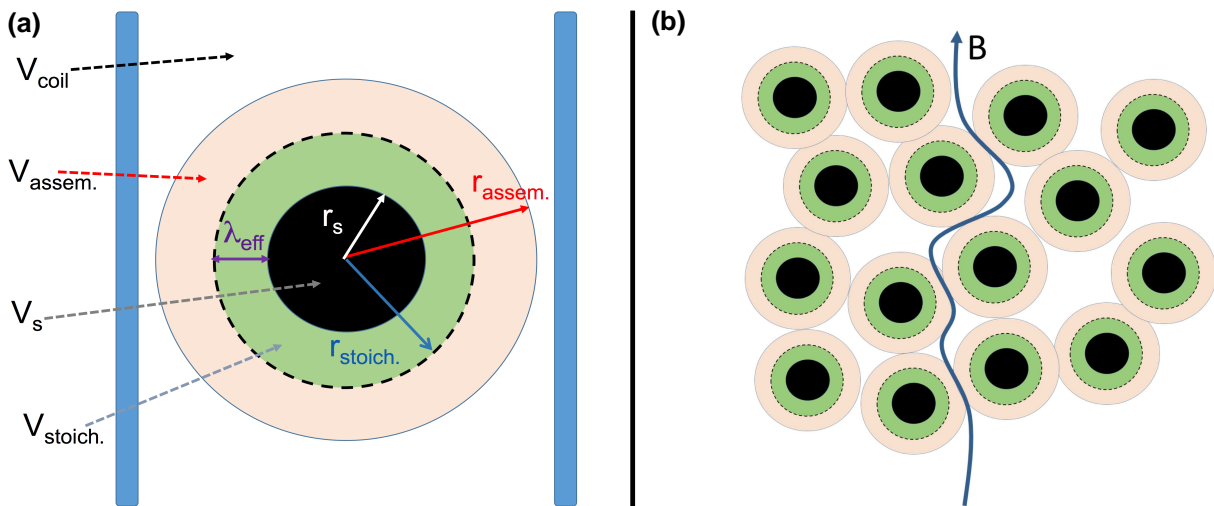
FIG. 5. Two scenarios for superconductivity in the nanoparticle assembly of $(TMTSF)_2ClO_4$: (a) Model of the nanoparticle assembly acting as a monolithic solid body in an inductive coil. (b) Visualization of magnetic field penetration in a weakly interacting assembly of superconducting nanoparticles.

1.2 K, where a quadratic field-dependent instrumental background present at all temperatures has been subtracted from the data. For $T < T_c$, δf_{norm} increases rapidly with field. For comparison, we show the normalized field dependent changes in susceptibility data, $\chi_{ave} = (2\chi_\perp + \chi_\parallel)/3$, averaged to estimate a random orientation from Ref. 21 for two similar temperatures (expanded view in lower inset). We find again a good qualitative similarity between the magnetic field dependent susceptibility of the nanoparticle assembly and bulk single crystal data. Quantitatively, the single crystal susceptibility data shows a slightly faster suppression of the diamagnetic shielding with field.

For higher fields δf_{norm} asymptotically approaches unity at different fields for different temperatures, which we interpret as the onset of the upper critical field H^*_{c2}. Given the uncertainties in estimating asymptotic intercepts, we have determined the H^*_{c2} onset vs. temperature for our complete set of field sweep data from - 2 T to 2 T (see Supplementary Figure 3[11]). The results are plotted in Fig. 7, along with previous determinations of H_{c2} by Murata et al.[25] for the three crystal directions, and their averaged (solid line) contribution. Clearly, H^*_{c2} of the NP-ClO_4 assembly follows closely the expectations for H_{c2} of the bulk crystal. We note that up to 16 T at 33 mK, there was no evidence for orbital features associated with the field induced SDW phases, nor the rapid oscillations[26]. Since these effects are periodic in inverse field for $B\|c$, they may average out due to the random nanoparticle orientations, although size effects may also play a role.

Summarizing, to the best of our knowledge the $(TMTSF)_2PF_6$ and $(TMTSF)_2ClO_4$ nanoparticle systems are the first assemblies of organic charge transfer metal nanoparticles to exhibit, respectively, a SDW formation and superconductivity. Our characterizations of
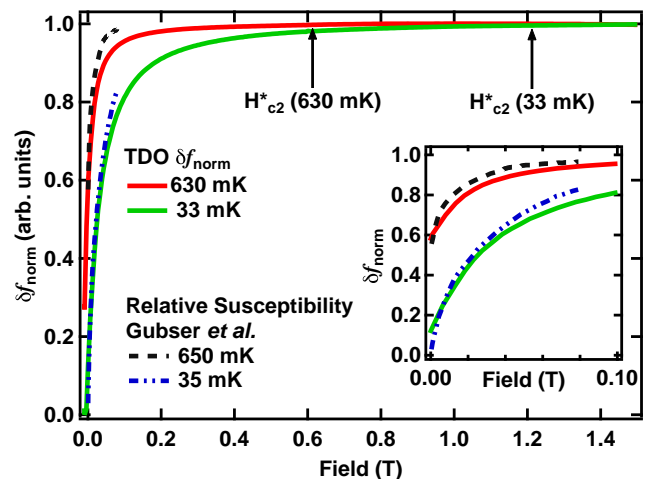

FIG. 6. A comparison of the magnetic field dependence of the normalized changes in the TDO frequency δf_{norm} (normalized with respect to $-\delta f$ at zero field for the lowest temperature sweep, 33 mK) compared with the normalized average relative susceptibility $\chi_{ave} = (2\chi_\perp + \chi_\parallel)/3$ obtained by Gubser et al.[21] (inset: expanded low field view). Estimates of the upper critical field H^*_{c2} (arrows) are obtained from the field where the signal asymptotically merges with the constant background at higher field. The randomly aligned nanoparticles exhibit a field dependence that is in qualitative agreement with the average response of aligned single crystals.

their ground state properties indicate a close correspondence to the bulk single crystal parent materials, and also give new information about the functional description of the nanoparticle structures beyond spectroscopy and electron microscopy. Specifically, the temperature dependent resistance measurements on $(TMTSF)_2PF_6$ indicate the presence of non-stoichiometric material that

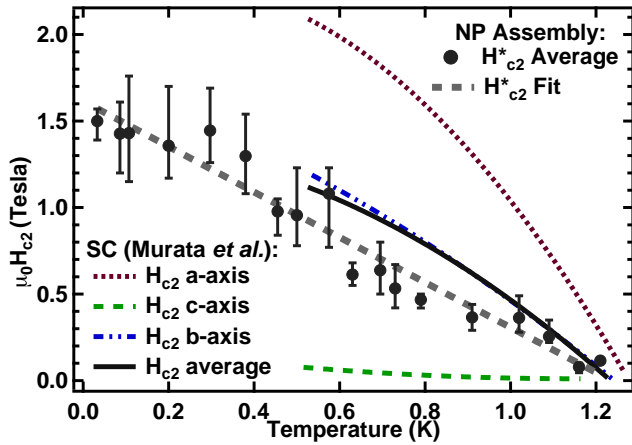FIG. 7. A comparison between the upper critical field H_{c2} reported on a single crystal (SC) of $(TMTSF)_2ClO_4$ for each axis (broken lines) and their average (solid line)[25] and our determination of H^*_{c2} for the $(TMTSF)_2ClO_4$ nanoparticle (NP) assembly (solid circles). The uncertainty-bars represent the range of H^*_{c2} values based on determinations from all field sweep data at each temperature. The gray-scale dashed line is a polynomial guide-to-the-eye fit, and indicates that H^*_{c2} for the $(TMTSF)_2ClO_4$ nanoparticle assembly is similar to that of H_{c2} for single crystals averaged over the three crystal directions.

we have modeled as a coating that in a nanoparticle assembly acts as both a series and parallel conducting path with the stoichiometric material. It is likely that the $(TMTSF)_2ClO_4$ functional structure is similar. Hence in the superconducting state, there are normal state regions between any two superconducting centers, and this will reduce the Josephson coupling in the assembly. The relatively large effective penetration depth $\Delta\lambda_{eff} \sim 150~\mu m$ may be a manifestation of this since the entire mass of the assembly is taken into account when estimating the nanoparticle effective volume, but only part of it actually goes superconducting and contributes to the change in diamagnetic shielding below T_c.

Based on the observations above, it is probable that the NP-ClO_4 act as isolated superconducting nano-sized regions below T_c. In this respect, previous work on Pb nanoparticles is instructive. Bulk Pb is a type I superconductor with a critical temperature of $T_c = 7.2$ K, a coherence length $\xi(0) \sim 90$ nm, and a penetration depth $\lambda(0) \sim 40$ nm. Li *et al.*[5] investigated both the susceptibility and resistivity of nanoparticle powders of Pb (NP-Pb) for a variety of nanoparticle sizes between 86 and 2 nm in capsules with a packing mass density of $\sim 7\%$ of the bulk (less than half of what we determined for our ClO_4 capsule). They found the T_c of NP-Pb did not decrease

until the particle size was less than 10% of the bulk coherence length. Two important implications of this work are that the NP-Pb act individually and not as a connected system, and that the nanoparticles must be significantly smaller in size than the coherence length before size effects cause a significant change in the superconducting order parameter.

III. CONCLUSIONS

The above experiments on nanoparticle Bechgaard salts, and the implications provided by comparisons with previous single crystal studies, are subject to a number of uncertainties, namely the distribution of nanoparticle sizes, the random orientation of the nanoparticles and experimental parameters including the relatively high frequency used (15 MHz – the quasiparticle skin depth above Tc is $\delta = 15~\mu m$ in the TDO probe). In spite of these complications, we find a remarkably strong correlation between the nano and bulk ground state properties, and the nanoparticle materials do indeed reflect the intrinsic materials with nearly unperturbed transition temperatures. Less clear is evidence for the nano-size effects on the temperature and magnetic field dependences of the ground states. Based on previous results on Pb nanoparticles, it may be necessary to significantly reduce the size of the $(TMTSF)_2ClO_4$ nanoparticles by an order of magnitude from 30 nm to 3 nm. Indeed, this is the size of the constituent nanoparticles that comprise a single nanoparticle (Fig. 1b). Future work will be needed to specifically address the effects of size on these constituent nanoparticles with, for instance, low temperature scanning probe spectroscopy.

* Corresponding Author: laurelewinter@gmail.com
† Corresponding Author: esteven@magnet.fsu.edu

[1] E. Abrahams, S. V. Kravchenko, and M. P. Sarachik, Reviews of Modern Physics **73**, 251 (2001).

[2] D. B. Haviland, Y. Liu, and A. M. Goldman, Physical Review Letters **62**, 2180 (1989).

[3] K. Ohshima, T. Kuroishi, and T. Fujita, J. Phys. Soc. Jpn. **41**, 1234 (1976).

[4] S. Bose, A. M. Garcia-Garcia, M. M. Ugeda, J. D. Urbina, C. H. Michaelis, I. Brihuega, and K. Kern, Nat Mater **9**, 550 (2010).

[5] W.-H. Li, C. C. Yang, F. C. Tsao, and K. C. Lee, Phys. Rev. B **68**, 184507 (2003).

[6] S. Reich, G. Leitus, R. Popovitz-Biro, and M. Schechter, Phys. Rev. Lett. **91**, 147001 (2003).

[7] J. Means, V. Meenakshi, R. V. A. Srivastava, W. Teizer, A. A. Kolomenskii, H. A. Schuessler, H. Zhao, and K. R. Dunbar, J. Magn. Magn. Mater. **284**, 215 (2004).

[8] K. Clark, A. Hassanien, S. Khan, K. F. Braun, and S. W. Hla, Nat. Nano **5**, 261 (2010).

[9] D. de Caro, L. Valade, C. Faulmann, K. Jacob, D. Van Dorsselaer, I. Chtioui, L. Salmon, A. Sabbar, S. El Hajjaji, E. Perez, S. Franceschi, and J. Fraxedas, New J. Chem. **37**, 3331 (2013).

[10] D. de Caro, C. Faulmann, L. Valade, K. Jacob, I. Chtioui, S. Foulal, P. de Caro, M. Bergez-Lacoste, J. Fraxedas, B. Ballesteros, J. S. Brooks, E. Steven, and L. E. Winter, European Journal of Inorganic Chemistry **2014**, 4010 (2014).

[11] See Supplementary Material at [ ] for additional nanoparticle photos, videos, and data.

[12] T. Ishiguro, K. Yamaji, and G. Saito, *Organic Superconductors*, 2nd ed. (Berlin, Heidelberg, New York:Springer-Verlag, 1998).

[13] P. Alemany, J.-P. Pouget, and E. Canadell, Phys. Rev. B **89**, 155124 (2014).

[14] The anisotropic properties of $(TMTSF)_2X$ are as follows[12] for the a, b and c-axis respectively. $(TMTSF)_2ClO_4$ - the lattice constants are 7.266 Å, 7.678 Å, and 13.275 Å; the transfer integrals are 250 meV, 25 meV, and 1.5 meV; the approximate coherence lengths at zero temperature are 800 Å, 300 Å, and 20 Å; the critical fields H_{c1}(50 mK) are 0.2 Oe, 1 Oe, and 10 Oe; and the upper critical fields H_{c2}(0 K) are 28 kOe, 21 kOe, and 1.6kOe. $(TMTSF)_2PF_6$ - the lattice constants are 7.297 Å, 7.711 Å, and 13.522 Å, and the transfer integrals are 0.51 meV, 0.52 meV and 1.73 meV.

[15] E. Steven, E. Jobiliong, P. M. Eugenio, and J. S. Brooks, Review of Scientific Instruments **83**, 046106 (2012).

[16] K. Mortensen, Y. Tomkiewicz, and K. Bechgaard, Phys. Rev. B **25**, 3319 (1982).

[17] W. A. Coniglio, L. E. Winter, K. Cho, C. C. Agosta, B. Fravel, and L. K. Montgomery, Phys. Rev. B **83**, 224507 (2011).

[18] G. J. Athas, J. S. Brooks, S. J. Klepper, S. Uji, and M. Tokumoto, Review of Scientific Instruments **64**, 3248 (1993).

[19] J.-P. Savy, D. de Caro, L. Valade, J.-C. Coiffic, E. S. Choi, J. S. Brooks, and J. Fraxedas, Synthetic Metals **160**, 855 (2010).

[20] J. P. Pouget, G. Shirane, K. Bechgaard, and J. M. Fabre, Phys. Rev. B **27**, 5203 (1983).

[21] D. U. Gubser, W. W. Fuller, T. O. Poehler, D. O. Cowan, M. Lee, R. S. Potember, L. Y. Chiang, and A. N. Bloch, Phys. Rev. B **24**, 478 (1981).

[22] R. Prozorov, R. W. Giannetta, J. Schlueter, A. M. Kini, J. Mohtasham, R. W. Winter, and G. L. Gard, Phys. Rev. B **63**, 052506 (2001).

[23] S. Haddad, S. Charfi-Kaddour, and J.-P. Pouget, Journal of Physics: Condensed Matter **23**, 464205 (2011).

[24] C. Kittel, *Introduction to Solid State Physics*, edited by 7th (New York: Wiley, 1996).

[25] K. Murata, M. Tokumoto, H. Anzai, K. Kajimura, and T. Ishiguro, Japanese Journal of Applied Physics **26**, 1367 (1987).

[26] S. Uji, T. Terashima, H. Aoki, J. S. Brooks, M. Tokumoto, S. Takasaki, J. Yamada, and H. Anzai, Phys. Rev. B **53**, 14399 (1996).